ACS SENSORS

pubs.acs.org/acssensors Article

Rapid and Sensitive Detection of *Mycobacterium tuberculosis* by an Enhanced Nanobiosensor

Jinbiao Ma, Manman Du, Can Wang,* Xinwu Xie,* Hao Wang, Tie Li,* Shixing Chen, Lixia Zhang, Shun Mao, Xiaohong Zhou,* and Min Wu

Cite This: *ACS Sens.* 2021, 6, 3367−3376 Read Online

ACCESS | Metrics & More | Article Recommendations | Supporting Information

ABSTRACT: Tuberculosis (TB) mostly spreads from person to person through *Mycobacterium tuberculosis* (MTB). However, the majority of conventional detection methods for MTB cannot satisfy the requirements for actual TB detection. As one of the most promising powerful platforms, a silicon nanowire field-effect transistor (SiNW-FET) biosensor shows good prospect in TB detection. In this study, an enhanced SiNW-FET biosensor was developed for the rapid and sensitive detection of MTB. The surface functional parameters of the biosensor were explored and optimized. The SiNW-FET biosensor has good sensitivity with a detection limit of 0.01 fg/mL toward protein. The current change value shows a linear upward trend with the increase in protein concentration in the range of 1 fg/mL to 100 μg/mL. One whole test cycle can be accomplished within only 30 s. More importantly, a good distinction was realized in the sputum without pretreatment between normal people and TB patients, which greatly shortened the TB detection time (only 2−5 min, considering the dilution of sputum). Compared with other methods, the SiNW-FET biosensor can detect MTB with a remarkably broad dynamic linear range in a shorter time.

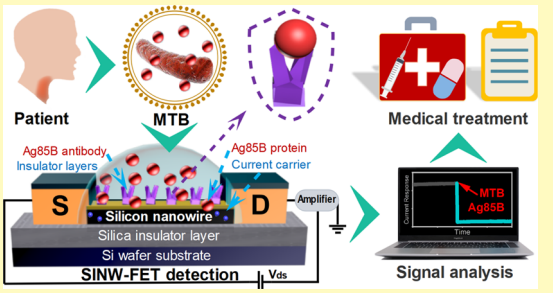

KEYWORDS: *Mycobacterium tuberculosis, sputum, silicon nanowire, field-effect transistor, biosensor*

Frequent outbreaks of airborne respiratory infectious diseases have rapidly and widely spread worldwide. Among them, tuberculosis (TB) has high morbidity and mortality as a chronic infectious disease mainly transmitted through the respiratory tract. "Global Tuberculosis Report 2020" from the World Health Organization (WHO) showed that approximately a quarter of the world's population has been infected by *Mycobacterium tuberculosis* (MTB). Approximately 10 million new cases of TB worldwide, 1.41 million deaths due to TB (the same in 2018), and nearly 2 billion people latently infected have been recorded in 2019.[1] Therefore, TB is still a public health threat that cannot be ignored.

Rapid and accurate detection is the basis for TB control. Bacteriological testing accounts for 80% of TB diagnoses.[1] TB mostly spreads from person to person through an MTB complex, particularly MTB.[2,3] However, MTB has strong resistance to harsh environments and can survive for a long time.[4] The present conventional detection methods for MTB mainly include culture method, imaging detection, sputum smear microscopy, tuberculin sensitivity test, serological detection, and molecular diagnosis.[5] Most of these techniques are complicated, are time-consuming, have low sensitivity, and require sophisticated equipment and high operational requirements, hence hindering their applications outside of controlled environments. The PCR-based GeneXpert recommended by WHO has significantly improved the detection efficiency of TB, but DNA samples need to be extracted. Moreover, it is expensive and restricted in developing countries.[6] In addition, the MTB concentration in environmental media is extremely low and difficult to detect, and impurities could cause interferences.[7,8]

To date, the rapid, efficient, and low-cost MTB detection remains a challenge. The development of biosensors in recent years provides a new strategy. Zhang et al. developed a piezoelectric sensor based on AuNPs combined with aptamer technology, which could detect MTB with a limit of 100 CFU/mL.[9] However, this method took 2 h to complete the detection. Bai et al. used a gold nanoparticle hybrid fullerene nanoparticle/nitrogen-doped graphene nanosheet biosensor to detect 3 fM MTB DNA; however, DNA extraction was a complex operation and was time-consuming.[10] Saengdee et al. developed an immunosensor based on a silicon nitrification ion-sensitive field-effect transistor (FET), which could detect 0.12 μg/mL MTB Ag85B protein within 1 h.[11] Although these

Received: June 10, 2021
Accepted: August 24, 2021
Published: September 2, 2021

biosensors have achieved good detection results compared with traditional methods, there is still room for improvement in detection performance to meet the needs of TB diagnosis. Among the recently emerging biosensors for MTB, nanobiosensors are a promising hotspot[12,13] because of their many advantages, such as high sensitivity and selectivity, fast analysis speed, label-free, simple operation, and low reagent consumption. Biosensors with active material in the nanoscale such as nanoparticles,[10] nanotubes,[14] nanosheets,[15] and quantum dots[16] are promising candidates for MTB detection and have achieved good results.

Among the diverse nanomaterial architectures, a silicon nanowire (SiNW) has exhibited substantial advantages due to its unique properties of one dimensionality and relatively standard processing techniques.[17,18] Its surface can be chemically functionalized and sensitively detect the absorbed biological/chemical substances via the change in conductivity. With the combined benefits of the well-developed silicon industry and the traditional complementary metal oxide semiconductor (CMOS) manufacturing technology, recent advancements in top−down fabrication technologies have paved the way to the large-scale production of high density and quality arrays of a SiNW-FET, a critical step toward their integration in real-life biosensing applications.[12] Hence, CMOS-compatible SiNW-FET sensing has a huge potential application.

Various SiNW-FET biosensors have been developed for a wide range of fields. When connected with different specific probes, these sensors can detect viruses,[19] proteins,[11] nucleic acids,[20] single cells,[21] tissues,[22] small molecules,[23] ions,[24] gases,[25] and other substances with high sensitivity and specificity. Shen et al. reported the selective detection of influenza A viruses down to 29 viruses/μL in clinical exhaled breath condensate samples (diluted by 100-fold) within minutes using SiNW sensor devices.[19] Gao et al. stated that this nanosensor can rapidly and sensitively detect as low as 1 fM DNA and is suitable for one-base mismatch discrimination. They physically engineered a SiNW with a back gate showing an optimized performance in low buffer ionic strength and at moderate probe concentration. Its DNA detection limit could be improved to 0.1 fM by operating in optimal conditions.[20,26] Shehada et al. used SiNWs to detect volatile organic compounds related to disease breathing and distinguish them to detect disease and estimate disease progression.[27] SiNWs are also used for the detection of other small molecules such as growth factor,[28] insulin,[29] dopamine,[30] TNT,[31] DMMP,[23] and uranyl.[32]

Although it is widely applied in microbial detection, the suitability of the SiNW for MTB detection still faces many challenges. The detection principle of the SiNW-FET biosensor is as follows: select the specific probe of the microorganism to be tested, functionalize the sensor surface, and perform detection.[25] SiNW-FET biosensors are often combined with immune technology to complete the detection. Techniques based on antigen−antibody interactions have been well established in biological research. One of the challenges is that the size of the MTB unit is beyond the Debye radius in the SiNW-FET biosensor.[33] Therefore, the direct ultrasensitive sensing of MTB cannot be achieved on the SiNW sensing platform.

Kesler et al. proposed two strategies, Debye volume and Debye time, in an attempt to break through the restriction of the Debye length on sensors.[34] Gao et al. used the SiNW-FET sensor supplemented with polyethylene glycol to detect prostate specific antigen under 15× PBS buffer solution.[35] Gutiérrez-Sanz et al. built a mixed-function layer using antibody fragments and polyethylene glycol, which increased the sensor's signal by 3-fold.[36] In this work, considering the convenience of operation and the cost of testing, the strategy is to select a specific MTB biomarker and an appropriate ion concentration in buffer so that the electrical signal generated by biological specific recognition is smaller than the Debye radius. This will not create a charge shield to ensure that the biosensor can perform sensitive detection.

In addition, the selected biomarker should be able to interact with the specific bioreceptor to form a stable complex through weak noncovalent bonds for target identification.[37] Therefore, small-scale identification elements for MTB must be screened. The antigen 85 (Ag85) complex is a major secreted protein in the filtrate of early MTB culture and accounts for 41% of the total protein.[38] The TB antigen Ag85B is the most abundant secreted protein of MTB with a molecular weight of 30 kD and can be detected in blood, urine, sputum, or cerebrospinal fluid.[39] Therefore, Ag85B can be used as a specific identification substance of MTB and combined with the SiNW-FET for TB detection.

The binding effect between the bioreceptor and the sensor surface also affects the detection performance of the sensor. Some researchers have adjusted and optimized the parameters of sensor surface functionalization to enhance the sensing performance. Su et al. used an external electric field to guide the direction when the antibody was fixed on the sensor. Atomic force microscopy was applied to measure the binding force of EEF to the target antigen under different angles. The largest binding force and current response were achieved at a certain angle.[40] Mirsian et al. improved the probe molecule immobilization process by changing the oxygen plasma (OP) processing conditions and the amount of water involved in the APTES reaction to achieve selective functionalization. Simulation and experimental results showed that the sensitivity of the sensor is three times higher that of biosensors based on nonselective functional design.[41]

At present, as a non-invasive sample, sputum has played an important role in the detection of TB. Sputum is a viscous mixture composed of cells and biochemical components of the peripheral airways and alveolar chambers, which appears in chronic respiratory diseases such as TB. It is by far the most frequent sample collected in the clinical laboratory for TB diagnosis and is widely used for microscopy and cytology research of infectious diseases.[42] The sputum composition includes primarily water (95%) and 5% solids that vary according to the disease (i.e., carbohydrates, lipids, DNA, filamentous actin, and proteoglycans),[43] which may affect the performance of the biosensor (i.e., hinder antibody−antigen interaction or cause nonspecific adsorption). The NALC-NaOH standard decontamination method for sputum samples is mostly used for processing. However, the operation is slightly troublesome, and pretreatment of them has a negative impact on the recovery of mycobacteria.[44] Therefore, to evaluate the diagnostic potential of the biosensor, we tested both the preprocessed sputum sample culture filter and the directly diluted sputum sample to evaluate the feasibility of the direct measurement of sputum samples.

Herein, a rapid and sensitive SiNW-FET biosensor for MTB detection was developed. For the first time, a CMOS-compatible SiNW-FET biosensor was proposed to detect

https://doi.org/10.1021/acssensors.1c01227
ACS Sens. 2021, 6, 3367−3376

MTB Ag85B protein, and its performance was fully evaluated. Surface functionalization parameters for the sensor were optimized to improve its performance. In particular, the optimization of plasma surface treatment, an important part of surface functionalization, greatly improved the detection of the sensor. The stability, detection limit, and specificity of the biosensor were tested and compared with those of other MTB Ag85B protein detection methods. Finally, the proposed strategy was applied to test sputum with TB, which greatly shortened the TB detection time. The prepared biosensor can be combined with a portable detector and can detect MTB in an actual environment.

EXPERIMENTAL SECTION

Materials. A 4 in. (111) silicon-on-insulator (SOI) wafer was acquired from Xinggui (SHH, CHN). Reagents for SiNW-FET-based modification preparation include the following: 3-aminopropyltriethoxysilane (APTES) (Abiocenter, BJ, CHN), ethanolamine (Kermel, TJ, CHN), glutaraldehyde (Xilong, GZ, CHN), phosphate buffer saline (PBS) tablet (Solarbio, BJ, CHN), and absolute ethanol (Bohua, TJ, CHN). All chemical reagents were of analytical grade and were used without further purification. Ag85B protein, anti-Ag85B, and carcinoembryonic antigen (CEA) were purchased from Abcam (USA). Ag85A, Ag85C, and H37Ra were obtained from Jingnuo (CHN). Bovine serum albumin (BSA) and IgG were bought from Solarbio (CHN). The proteins were used without further purification and diluted to desired concentrations with the assay buffer. The MTB H37Rv culture medium for patients with TB was provided by Haihe Hospital. MTB Ag85B ELISA Kit was bought from Meimian (JS, CHN).

SiNW-FET Fabrication. A high-response 160-SiNW array was fabricated on a (111) SOI wafer by the CMOS-compatible microfabrication technology. SiNW-FET fabrication steps are shown in Figure 1. A SiNW was prepared following the "top−down" method, including anisotropic etching and self-limiting oxidation, on a (111) SOI wafer.[45] A SiNW with an inverted triangle shape was generated at the top center of the wall beneath the silicon nitride layer, which has the largest surface-to-volume ratio and depletion ratio to significantly enhance the sensors' sensitivity.[46] The doping windows were etched at designed source and drain locations, and boron was doped at the window position to form good ohmic contact between silicon and metal. Then, it was packaged on the PCB board and further packaged as a SiNW-FET biosensor.

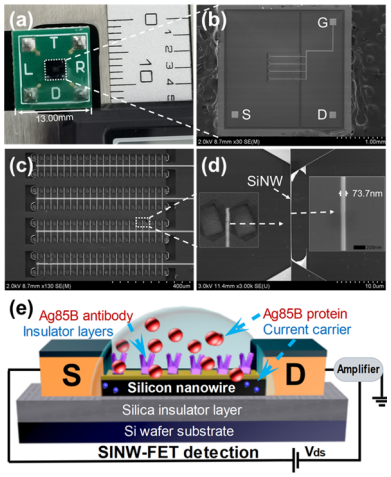

Figure 1. SiNW-FET interface characterization and performance test. (a) Image of the packaged device. (b) SEM of the SiNW-FET device. (c) SEM of a silicon nanowire array region. (d) SEM of the silicon nanowire in the schematic diagram of the SiNW-FET device. (e) Schematic diagram of the SiNW-FET biosensor detection principle.

As shown in Figure 1a, the packaged sensor size is only 13 mm by 13 mm and is flexible and portable. A scanning electron microscope was used to characterize the different dimensions of the biosensor surface. As shown in Figure 1b,c, gold was used as a contact metal and leading wires, and 160 well-ordered SiNWs were arranged on a chip as a sensing element. As shown in Figure 1d, the SiNWs on the inner wall of the pit were covered by an oxide layer on the surface. SEM was used to characterize the oxide layer on the etched SiNW surface and revealed that its width was small at only 73.7 nm. Given that the SiNW with a small diameter has a large surface-to-volume ratio, the dimension of NWs would play an important role in the transport properties.

Each surface ion was assumed to contribute a carrier to the SiNW, and the excess carriers were homogeneously distributed in NWs due to the nanoscale size of the latter. As a result, the relation between the total conductivity (σ_{nw}) and diameter (d) of NW is given by

$$\sigma_{nw} = \left(n_0 + \frac{4n_s}{d}\right) q\mu_h \tag{1}$$

where n_0 is the carrier concentration that NWs inherit from the original Si wafer, n_s is the density of surface ions, and μ_h is the carrier mobility.[47] Carrier mobility is estimated in the Supporting Information. We put σ_{nw} = 2.4 s/cm, $n_0 = 1 \times 10^{15}$ cm^{-3}, $d = 73.7 \times 10^{-7}$ cm, and μ_h = 450 cm^2/(V·s) into the above equation to get the expected value $n_s = 5.9 \times 10^{10}$ cm^{-2}, which is close to the result using the nanosensor-measured value (1.9×10^{10} cm^{-2}). Equation 1 shows that when the size is extremely small, the influence of surface ions on its transmission performance becomes dominant. Within a certain range, the high value of n_s/d would lead to high conductivity, which accordingly increased the response of the sensor signal. However, the small size of the nanowire would result in great noise interference. Therefore, a balance should be made between the above two sides. Therefore, the sensor can detect low-concentration surface ions with high sensitivity.

Detection Principle. As shown in Figure 1e, MTB-specific bioreceptor anti-Ag85B antibody was immobilized on the SiNW as the gate of FET. FET-based immunosensing technology (immunoFET) converts the generated biological signal into the current change of the FET by binding the target biomolecule Ag85B.[48,49] When an antibody (Ab) with charge X_1 undergoes an immunological reaction with an antigen (Ag) with charge X_2, an antibody−antigen complex with a total charge X_3 is formed.

$$Ab^{X_1} + Ag^{X_2} \overset{K}{\Leftrightarrow} [AbAg]^{X_3} \tag{2}$$

The charge difference from X_1 to X_3 can be measured by the immunoFET. The charge density change at the gate oxide/solution interface induces the same change but an opposite sign at the semiconductor/oxide interface, thus affecting the threshold voltage of the immunoFET.[37] Under a constant source voltage, the current response of applying a varying gate voltage (simulating SiNW surface charge density change) changes accordingly. See Figure S1, Supporting Information, for details.

The influence of Debye shielding on charge detection in the solution must be considered. When a certain distance is exceeded, the charge change in biometric recognition cannot be detected. As shown in eq 1, Debye shielding mainly acts in n_s when the size of charged macromolecules exceeds the Debye radius. The generated Debye shielding would make n_s stable even when biological specific recognition generates electrical signals. Therefore, σ_{nw} will remain stable. The Debye length (λ_D) quantifies this screening length and is defined as:

$$\lambda_D = \sqrt{\frac{\varepsilon kT}{e^2 \sum_i N_A c_i z_i^2}} \tag{3}$$

where e is the proton charge, ε is the permittivity of the solvent, N_A is Avogadro's number, z_i and c_i are the valence and concentration of ion

https://doi.org/10.1021/acssensors.1c01227
ACS Sens. 2021, 6, 3367−3376

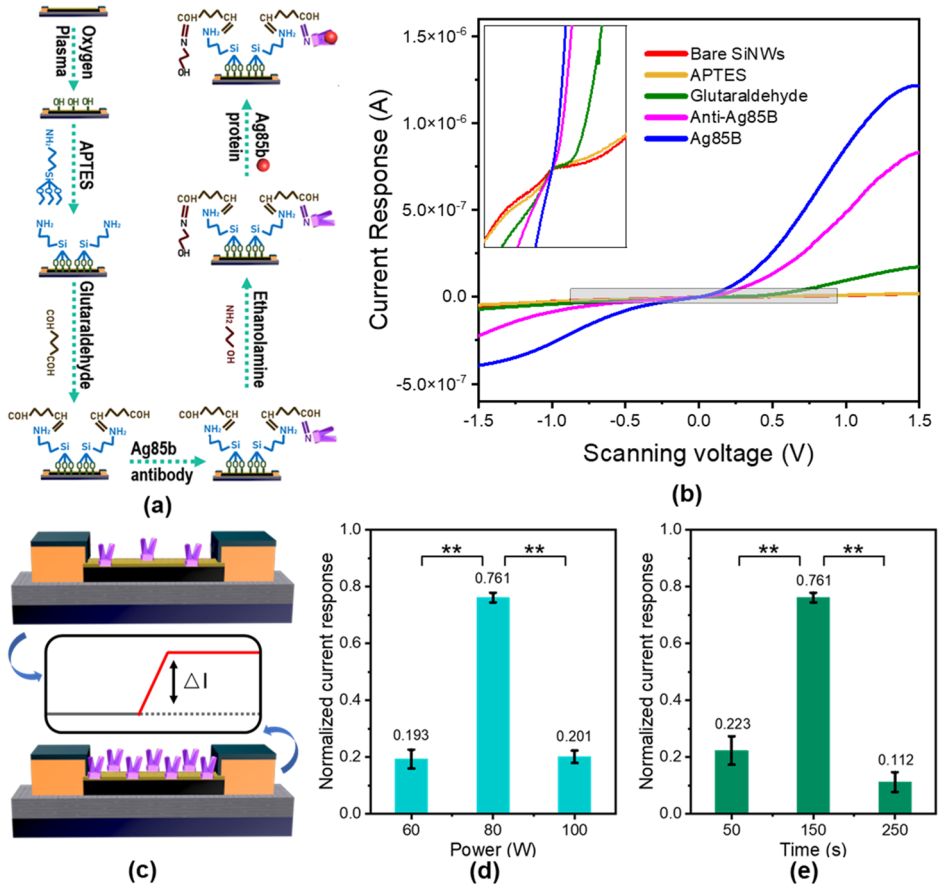

Figure 2. Surface modification of the SiNW-FET biosensor. (a) Surface modification steps of the SiNW-FET biosensor. (b) Electrochemical characterization of the modification process. (c) Relationship between sensor surface functionalization and detection sensitivity. (d) Processing times of 50, 150, and 250 s under 80 W power condition. (e) Power conditions of 60, 80, and 100 W under 150 s processing time; the effect of plasma parameter adjustment was analyzed using 1 μg/mL Ag85B protein. Double asterisk (**) means that the difference between the two groups of data is extremely significant (p = 0.05). Each data set displayed the average and standard deviation (SD) of the results from three independent experiments (n = 3).

species i, respectively, and the sum extends over all ion species in solution.[50] An appropriate salt concentration of the buffer for biological detection must be selected to ensure that λ_D is sufficiently long to allow sensing but short enough to screen unbound macromolecules.[51] For high electrolyte concentrations, the low-frequency noise of the FET dominates over the electrolyte noise; hence, the electrolyte concentration should be reduced to achieve high sensitivity.[52] Sensing measurements were performed in diluted buffer solutions to circumvent the obstacle of the Debye length.

According to charge shielding, a large Debye radius is suitable for molecular detection. However, an extremely low ion concentration can potentially affect protein conformation and result in the subsequent loss of protein activity and binding affinity because the protein structure is highly dependent on environmental conditions supplied by its solvent.[53] In addition, when the PBS concentration is too low, the pH value of the solution will be unstable, which will lead to unstable electrochemical signals.[54] Calculation results revealed that the Debye radius of 0.01× PBS is 7.3 nm,[55] which is suitable for the electrical signal detection of general biological macromolecules.

The molecule radius of Ag85B can be estimated by this equation:

$$a = 0.33M^{0.46} \quad (4)$$

where a represents the molecule radius (Å), and M represents the molecule weight.[56] Ag85B is a protein with a molecular weight of 30 kD. According to this equation, the Ag85B protein size is 3.78 nm. The Ag85B antibody belongs to the IgG type, and the height of the IgG immobilized on the silicon dioxide surface is reported to be 4 nm.[57] Therefore, the charge of the protein at the farthest position of the SiNW (3.78 nm) plus the size of the antibody (4 nm) is nearly equivalent to the 0.01× PBS Debye radius (7.3 nm). These theoretical results suggest that the Debye shielding possibly does not affect the sensing.

After preliminary tests, 0.01× PBS was determined as the optimal concentration of the balance between the two aspects, confirming the conclusion inferred previously. More details can be found in Figure S2, Supporting Information.

Surface Functionalization. The SiNW-FET functionalization process is shown in Figure 2a. Under atmospheric conditions, a natural oxide layer was formed on the SiNW surface. Prior to modification, the SiNW sensor was pretreated with oxygen plasma to clean up any organic contamination and generate −OH groups on its surface. The treated chips were immediately used after OP treatment to prevent surface degradation. The parameters of plasma treatment, an important part of sensor functionalization, were adjusted and optimized. The final conditions were 80 W and 150 s. The biosensor was entirely immersed in APTES solution (2% ethanol) overnight to form primary amino groups on the sensing NW surface and then treated at 120 °C for 15 min to stabilize the functional groups. A biofunctional linker, glutaraldehyde, was then covalently attached onto the amine-terminated surface by immersing the chip in a solution of 25% glutaraldehyde in buffer solution (1× PBS) for 2.5 h. Antibody attachment on the SiNW surface was conducted by exposing the SiNW to 133 μg/mL antibody against Ag85B (anti-Ag85B) (1× PBS) for 2.5 h. Nonspecific sites were blocked with 100 mM ethanolamine solution (1× PBS) to reduce the nonspecific absorption of the surface. After each modification step was completed,

https://doi.org/10.1021/acssensors.1c01227
ACS Sens. 2021, 6, 3367−3376

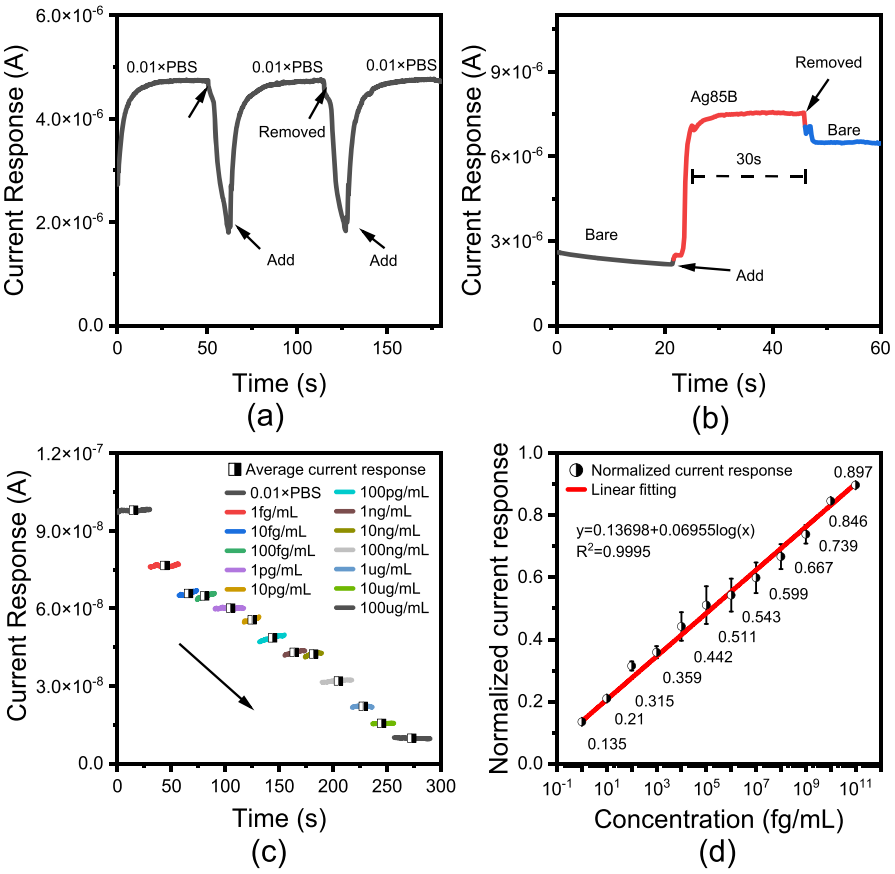

Figure 3. Performance test of the SiNW-FET biosensor. (a) Reproducibility and stability test of the SiNW-FET biosensor and (b) single response−recovery test of the SiNW-FET biosensor to Ag85B. (c) The SiNW-FET detects the current response of the concentration gradient Ag85B protein in PBS buffer. (d) Normalized curve of telecommunication response with the Ag85B concentration gradient. Each data set displayed the average and SD of the results from three independent experiments (n = 3).

the same buffer was used for rinsing and the sensor was blow-dried with nitrogen. All steps were performed at room temperature except for the instructions in advance.

As shown in Figure 2b, a scanning voltage of 1.5 to −1.5 V (points: 300) was used between the source and the drain to electrochemically characterize each modification step. As the modification progressed, the current response exhibited an increasing trend within the positive voltage range. Therefore, modification successfully changed the electrochemical characteristics of the sensor as confirmed by the different scanning curves.[23] At the same time, we measured the transfer characteristic curve of the sensor at different gate voltages (Figure S3, Supporting Information) and different PBS concentrations (Figure S4, Supporting Information).

Sensing Apparatus and Parameters. For Ag85B sensing measurement, a Keithley 2400 semiconductor parameter analyzer was used to read and process the signal generated by the SiNW array chip. This device was placed in a cassette with the same external environmental factors, and 0.3 V voltage was applied between the source and the drain of the biosensor and the drain current was also measured. The gate voltage was grounded, which can be considered as 0 V. The same source and gate voltage were used in a previous publication.[31] Prior to the test, PBS buffer was trickled on the sensor for several minutes until the baseline current stabilized. Afterward, 7 μL of samples was sequentially added while monitoring the real-time current signal. The signal must first stabilize before the unreacted sample is removed, and the next sample must be added after the signal stabilizes again. The sensing performance was tested at room temperature. The target current was monitored in the whole process.

For comparison between biosensors, the current change was normalized. The normalized current response was calculated according to the following equation:

$$\text{normalized current response} = \frac{\Delta I}{I_0} = \frac{I_0 - I_t}{I_0} \quad (5)$$

where I_t is the source−drain current at a given time point during the Ag85B protein measurement in real time, and I_0 is the 0.01× PBS buffer current measured without the sample.

RESULTS AND DISCUSSION

Optimization of Surface Functionalization Parameters. The parameters processed by OP were explored and optimized. One of the efficient ways to improve the sensitivity of SiNW is to increase the number of absorption sites for specific binding of proteins on the surface of the nanowires.[25] Figure 2c shows that within a certain degree of the sensor, the change value of the current signal increases with the numbers of antibodies fixed on the SiNW-FET surface. Therefore, the performance of the sensor can be improved by increasing the binding rate of the antibody and the surface. Plasma can generate −OH functional groups on the sensor surface for subsequent antibody immobilization. The normalized current response of 1 μg/mL Ag85B solution was used to characterize the effect of plasma parameter adjustment. Figure 2d shows the current response under 80 W power and processing times of 50, 150, and 250 s. Analysis results reveal that under 150 s, the normalized current response to Ag85B protein is significantly higher than those under other processing conditions. Figure 2e shows the normalized current response to Ag85B protein under 150 s processing time with processing power of 60, 80,

https://doi.org/10.1021/acssensors.1c01227
ACS Sens. 2021, 6, 3367−3376

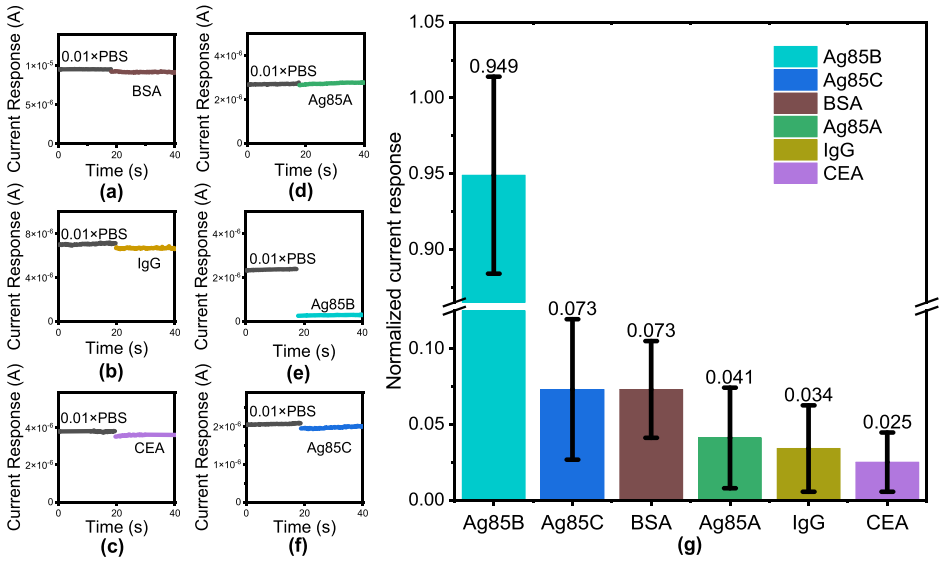

Figure 4. Specificity of the biosensor for the detection of six kinds of proteins. Current response of SiNW-FET to 10 ng/mL (a) BSA, (b) IgG, (c) CEA, (d) Ag85A, (e) Ag85B, and (f) Ag85C; six 10 ng/mL proteins were added to the sensor. (g) Normalized response curves of six proteins. Each data set displayed the average and SD of the results from three independent experiments (n = 3).

and 100 W. Under 80 W, the normalized current response to Ag85B protein is significantly higher than those under other processing conditions. A single-factor significance analysis was performed on the adjustment results of the above four parameters. Table S1, Supporting Information, shows that the p values are all less than 0.01; hence, the normalized current response difference is extremely significant after parameter adjustment.

Only when the thickness of silicon oxide is close to zero can the SiNW obtain sensing properties.[58] Plasma treatment can perform dual effects of physical bombardment and chemical reaction of the oxide layer on the surface silicon wafer through active plasma. Hydroxyl groups appear on the sensor surface and facilitate the subsequent antibody immobilization.[59] Its processing effect is positively related to processing power and time. When the power is low and the processing time is short, the sensor produces less hydroxyl groups. Insufficient surface activation results in a small number of antibody connections; hence, the normalized current response is small. On the contrary, when the processing power is high and the time is long, the surface of the sensor will be over-etched, thus affecting the structure of the SiNW and producing a small normalized current response.[41]

Stability and Response Time. The prepared SiNW device in this study presents good homogeneity and stable performance, which can refer to our recent publication.[48] Briefly, 0.01× PBS was drizzled three times on the sensor and then removed. As shown in Figure 3a, the current signal is basically the same, thus proving that the sensor and the selected buffer have good stability. The detection speed of the sensor was also tested. Figure 3b shows that the current signal increased sharply when Ag85B was added on the empty sensor but decreased after the sample was removed. The sensor can complete 100 μg/mL Ag85B detection in 30 s, indicating its good stability and short response time.

Sensitivity and Detection Limit. Briefly, 0.01× PBS buffer was used to dilute Ag85B protein from 100 μg/mL to 1 fg/mL with a 10-fold concentration gradient. Afterward, 7 μL of samples from low to high concentration was sequentially added to the surface of the SiNW-FET. The sample was repeatedly blown with a pipette gun to reduce the diffusion time. For the convenience of observation, we intercept the data during the stationary phase of the sensor signal. We recorded the reaction kinetic curves of 1 fg/mL and 100 μg/mL Ag85B protein (Figure S5, Supporting Information). This result accords with the reaction kinetics: the higher the protein concentration, the faster the binding rate.[25] Figure 3c shows that with the increase in concentration, the electrical signal shows a downward trend. This phenomenon can be explained by the binding of Ag85B protein and Ag85B antibody. Given that the prepared sensor is p-doped, the binding of charged substances to the sensor surface induces the transfer of carriers and changes the signal. Hence, SiNW conductance is modulated by an applied voltage, and the positively charged Ag85B protein bound on the SiNW surface can modulate their conductance by changing the thickness of the hole accumulation layer.[25] In this case, the adsorbed proteins may act as chemical gates that shift the Fermi level of the SiNW in the upper part of the band gap and increase the resistance of the device, thus reducing the signal. When the protein concentration increases, the unbound Ag85B antibody recognition sites are gradually filled. Therefore, the current signal continuously drops.[33]

The data must be normalized due to differences in the electrochemical performance of biosensors. As shown in Figure 3d, normalized fitting was performed on the telecommunication response change value of the Ag85B concentration gradient. The normalized current response has a linear relationship with the logarithm of the Ag85B concentration. The current change value shows a linear upward trend with increasing Ag85B concentration in a range of 12 dilution concentration gradients (1 fg/mL to 100 μg/mL). Chen et al. developed an NW-based EGFET that exhibits excellent performance, which can detect DNA in a range of 13 concentration gradients (10^{-19} to 10^{-6} M).[60] The detection limit of the SiNW-FET for Ag85B protein can reach 1 fg/mL. Sensitivity values were obtained from the slope of the linear fit and can be applied to the dose−response curves. As shown in

https://doi.org/10.1021/acssensors.1c01227
ACS Sens. 2021, 6, 3367−3376

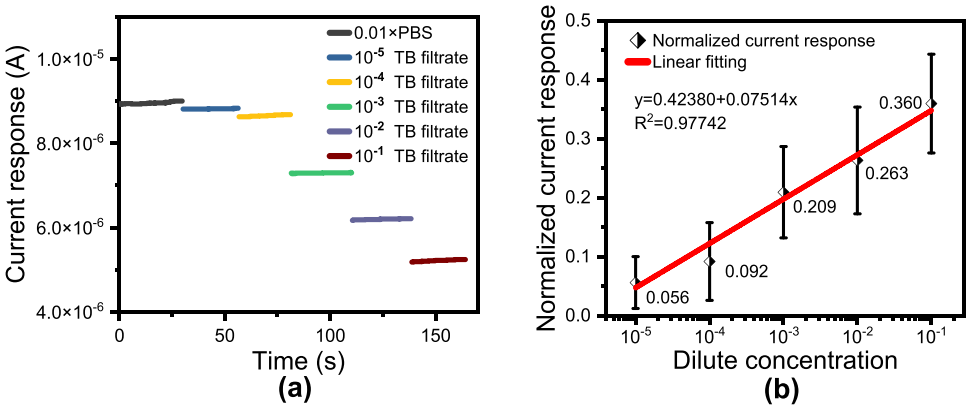

Figure 5. Detection of sputum culture fluid. (a) The SiNW-FET detects the current response of the concentration gradient filtrate of patients with TB in PBS buffer. (b) Normalized curve of telecommunication response with the filtrate of patients with a TB concentration gradient. Each data set displayed the average and SD of the results from three independent experiments (n = 3).

Figure S6, Supporting Information, the current signal response sensitivity of the sensor is 5.96 nA/log(fg/mL). A linear response range from 1 fg/mL to 100 μg/mL toward Ag85B protein was obtained for the SiNW-FET biosensing platform. The signal generated by 0.01× PBS buffer was selected as the background signal, and three times the standard deviation of its current response were inputted into the above linear fitting formula. The limit of detection (LOD) was 0.01 fg/mL.

Specificity. Five 10 ng/mL proteins were used for anti-interference detection to test the specificity of the sensor. Three common proteins (BSA, IgG, and CEA) and two proteins (Ag85A and Ag85C) similar to Ag85B were used for specificity control experiments. As shown in Figure 4g, the signal change of Ag85B was approximately 0.95, and those of the other proteins were all lower than 0.1. The sensor's signal response to Ag85B was significantly higher than those of the other five proteins. These results show that the SiNW-FET biosensor has good specificity for Ag85B compared with other investigated proteins, can effectively avoid unspecific binding, and thus has ultrahigh specificity.

Detection of Sputum Culture Fluid. To evaluate the diagnostic capability of the biosensor, we tested the preprocessed sputum sample culture filtrate. As mentioned earlier, the antigen 85 complex is a major secreted protein in the filtrate of early MTB culture.[38] Sputum was collected from patients with TB for culture. However, impurities in the sputum may affect the performance of the biosensor. We first adopt the NALC-NaOH standard decontamination method for digestion, decontamination, and concentration treatment. Then, following Phunpae et al.'s method,[61] the sputum culture fluid was filtered through a 0.22 μm filter and diluted with 0.01× PBS buffer to obtain five concentration levels.

As shown in Figure 5a, the current response signal decreases when the filtrate concentration increases. As shown in Figure 5b, the normalized current response of the sensor has a linear relationship with the filtrate of samples diluted with a concentration gradient of 10^{-5} to 10^{-1} and its slope value is similar to the Ag85B protein in Figure 3d. Compared with pure Ag85B protein, the filtrate of patients with TB has larger error bars due to the presence of other interfering substances. We take the normalized current response value of 0.360 of the sample diluted 10 times into the fitting formula in Figure 3d, and the Ag85B protein concentration of the sample is calculated to be 15.8 pg/mL. The result was also verified using the ELISA kit, with a protein concentration of 27.9 pg/mL, which is close to the result using the nanosensor detection (15.8 pg/mL). However, ELISA is also time-consuming and requires 5 h. Therefore, the prepared sensor can rapidly detect the Ag85B protein secreted by MTB in the actual clinical samples.

Detection of Unprocessed Sputum. Although we have achieved good results using sputum culture fluid, the pretreatment and culture of sputum are time-consuming, which cannot be combined with the high specificity, high sensitivity, and rapidity of the SiNW-FET biosensor. Therefore, we used biosensors to directly test unprocessed sputum samples to investigate the diagnostic potential of biosensors. Sputum samples from TB patients contain MTB that secretes the Ag85B protein. But they also contain more impurities, which will affect the sensitivity of the biosensor, so the sputum needs to be diluted.

We collected positive sputum samples from three TB patients and negative sputum samples from normal people and diluted them to 10^{-4} times. Three positive sputum samples were certified by the BECTEC MGIT 960 system to contain MTB. The normalized current response is shown in Figure 6. The results show that our sensor can distinguish between negative and positive TB samples, which greatly shortened the

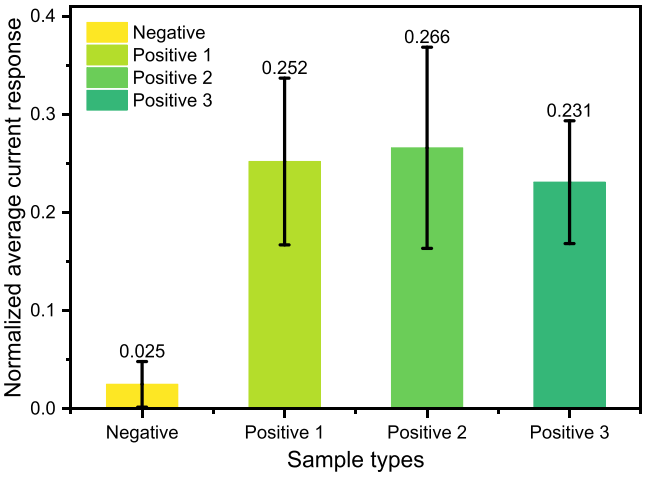

Figure 6. Normalized current response graph of negative and positive sputum samples. Each data set displayed the average and SD of the results from two independent experiments (n = 2).

https://doi.org/10.1021/acssensors.1c01227
ACS Sens. 2021, 6, 3367−3376

TB detection time (only 2−5 min, considering the dilution of sputum). The rapid diagnosis of TB is particularly important for the prevention and control of TB, and the effect of our program is encouraging. Although more data are needed to confirm the feasibility of the application of this biosensor in actual detection, we undoubtedly propose a new idea that can be applied to the preliminary screening of TB patients.

Comparative Sensitivity and Practical Applicability. Some technologies have been developed to detect MTB Ag85B. The detection results are summarized in Figure 7, and

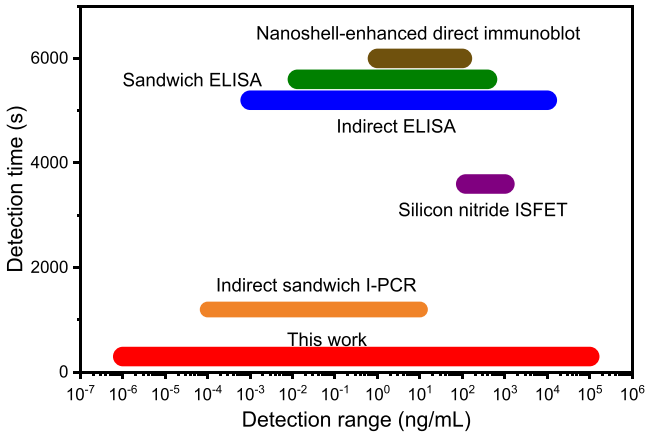

Figure 7. Comparison of different biosensing techniques for MTB Ag85B detection.

specific data are listed (Table S2, Supporting Information). The results show that the proposed method can complete the detection in a short time. Its detection effect is more sensitive than those of other technologies, and its dynamic range covers more than 12 orders of magnitude. Therefore, this strategy can be used to detect actual clinical samples with a wide range of MTB Ag85B concentrations. Indeed, the difference between the actual sample and the ideal sample is reflected in the detection range and the error bar. Compared with pure Ag85B protein (Figure 3d), the filtrate of patients with TB (Figure 5b) has larger error bars and a smaller detection range due to the presence of other interfering substances.

CONCLUSIONS

An enhanced SiNW-FET biosensor for Ag85B detection was developed for rapid and sensitive MTB detection. The main secreted protein Ag85B of MTB was selected as the identification element. The surface functional parameters of the biosensor were explored and optimized. Its LOD for MTB Ag85B is as low as 0.01 fg/mL (0.33 aM) with good specificity and stability and response within 30 s. The large dynamic range of this sensor spans 12 orders of magnitude from 1 fg/mL to 100 ng/mL or even higher, thus offering an opportunity to detect a broad scope of MTB concentrations in actual clinical and environmental samples. Anti-interference tests with other proteins revealed good results. Its normalized current response to Ag85B exceeds 0.9, whereas those of other related proteins are less than 0.1. Compared with other methods, the SiNW-FET biosensor only needs a small amount of sample (7 μL) and can detect MTB with a remarkably broad dynamic linear range in a shorter time.

The analysis of sputum culture fluid from patients with TB indicated that the sensor has a linear relationship with 5 orders of magnitude of diluted samples, thus confirming its applicability for TB detection in an actual environment. A good distinction was realized in the sputum without pretreatment between normal people and TB patients, which greatly shortened the TB detection time (only 2−5 min, considering the dilution of sputum). The rapid and sensitive detection of MTB plays a key role in the treatment of personal diseases and the control of TB. Compared with the ELISA method, this research can complete the detection in a shorter time. Although more data may be needed to confirm the method we have established for the early diagnosis of TB, our results are encouraging and are of great significance for the rapid detection of TB and the control of the prevalence of TB.

ASSOCIATED CONTENT

Supporting Information

The Supporting Information is available free of charge at https://pubs.acs.org/doi/10.1021/acssensors.1c01227.

Estimation of the mobility, current response under scanning gate voltage, determination of Ag85B protein at different PBS concentrations, electrochemical characterization at different gate voltages, electrochemical characterization at different PBS concentrations, real-time response curves of different concentrations of Ag85B protein, fitting diagram of the average current response with the concentration of gradient protein, significance analysis table of plasma parameter optimization, and performance comparison table of different detection methods for MTB Ag85B (PDF)

AUTHOR INFORMATION

Corresponding Authors

Can Wang − *School of Environmental Science and Engineering, Tianjin University, Tianjin 300072, PR China; Tianjin Key Lab of Indoor Air Environmental Quality Control, Tianjin 300072, PR China;* orcid.org/0000-0003-3575-5975; Email: wangcan@tju.edu.cn

Xinwu Xie − *Institute of Medical Support Technology, Academy of Military Science, Tianjin 300161, PR China; National Bio-Protection Engineering Center, Tianjin 300161, PR China;* orcid.org/0000-0002-6446-4045; Email: xinwuxie@163.com

Tie Li − *Science and Technology on Micro-system Laboratory and State Key Laboratories of Transducer Technology, Shanghai Institute of Microsystem and Information Technology, Chinese Academy of Sciences, Shanghai 200050, PR China;* orcid.org/0000-0001-9907-0188; Email: tli@mail.sim.ac.cn

Xiaohong Zhou − *State Key Joint Laboratory of ESPC, School of Environment, Tsinghua University, Beijing 100084, PR China;* orcid.org/0000-0002-5307-6709; Email: xhzhou@mail.tsinghua.edu.cn

Authors

Jinbiao Ma − *School of Environmental Science and Engineering, Tianjin University, Tianjin 300072, PR China; Tianjin Key Lab of Indoor Air Environmental Quality Control, Tianjin 300072, PR China;* orcid.org/0000-0001-6142-6708

Manman Du − *School of Environmental Science and Engineering, Tianjin University, Tianjin 300072, PR China;*

https://doi.org/10.1021/acssensors.1c01227
ACS Sens. 2021, 6, 3367−3376

Tianjin Key Lab of Indoor Air Environmental Quality Control, Tianjin 300072, PR China

Hao Wang − *Institute of Medical Support Technology, Academy of Military Science, Tianjin 300161, PR China; School of Electronic Information and Automation, Tianjin University of Science and Technology, Tianjin 300222, PR China*

Shixing Chen − *Science and Technology on Micro-system Laboratory and State Key Laboratories of Transducer Technology, Shanghai Institute of Microsystem and Information Technology, Chinese Academy of Sciences, Shanghai 200050, PR China*

Lixia Zhang − *Tianjin Haihe Hospital, Tianjin 300350, PR China*

Shun Mao − *College of Environmental Science and Engineering, Tongji University, Shanghai 200092, PR China;* orcid.org/0000-0003-3319-4203

Min Wu − *Tianjin Haihe Hospital, Tianjin 300350, PR China*

Complete contact information is available at: https://pubs.acs.org/10.1021/acssensors.1c01227

Author Contributions

J.M. conceived the study, designed and performed experiments, analyzed data, and wrote the manuscript. C.W. and X.X. conceived the study, obtained funding, and revised the manuscript. M.D., H.W., S.M., and X.Z. revised the manuscript. T.L. and C.X designed the biosensor. L.Z. and M.W obtained the TB sample. All authors contributed to the writing of the manuscript and the analysis of data.

Notes

The authors declare no competing financial interest.

■ ACKNOWLEDGMENTS

This research was supported by the Key Technologies R&D Program of Tianjin (20ZXGBSY00100), National Key Research and Development Program of China (no. 2017YFA0207103), National Natural Science Foundation of China (grant no. 51678402), National Science and Technology Major Project (2017ZX10304403-003-004), and National Natural Science Youth Foundation (grant no. 31900937).

■ REFERENCES

(1) World Health Organization *Global tuberculosis report 2020*; World Health Organization, 2020, https://www.who.int/teams/global-tuberculosis-programme/data (Update 14 Oct 2020).

(2) Patterson, B.; Wood, R. Is cough really necessary for TB transmission? *Tuberculosis* **2019**, *117*, 31−35.

(3) CDC *Basic TB Facts*; Centers for Disease Control and Prevention: 2016. http://www.cdc.gov/tb/topic/basics/.

(4) Frieden, T. R.; Sterling, T. R.; Munsiff, S. S.; Watt, C. J.; Dye, C. Tuberculosis. *Lancet* **2003**, *362*, 887−899.

(5) Gupta, S.; Kakkar, V. Recent technological advancements in tuberculosis diagnostics - A review. *Biosens. Bioelectron.* **2018**, *115*, 14−29.

(6) Singh, N.; Sreenivas, V.; Gupta, K. B.; Chaudhary, A.; Mittal, A.; Varma-Basil, M.; Prasad, R.; Gakhar, S. K.; Khuller, G. K.; Mehta, P. K. Diagnosis of pulmonary and extrapulmonary tuberculosis based on detection of mycobacterial antigen 85B by immuno-PCR. *Diagn. Microbiol. Infect. Dis.* **2015**, *83*, 359.

(7) Jones-López, E. C.; Acuña-Villaorduña, C.; Ssebidandi, M.; Gaeddert, M.; Kubiak, R. W.; Ayakaka, I.; White, L. F.; Joloba, M.; Okwera, A.; Fennelly, K. P. Cough aerosols of *mycobacterium tuberculosis* in the prediction of incident tuberculosis disease in household contacts. *Clin. Infect. Dis.* **2016**, *63*, 10−20.

(8) Wang, Y.; Wang, C.; Song, L. Distribution of antibiotic resistance genes and bacteria from six atmospheric environments: Exposure risk to human. *Sci. Total Environ.* **2019**, *694*, 133750.

(9) Zhang, X.; Feng, Y.; Duan, S.; Su, L.; Zhang, J.; He, F. *Mycobacterium tuberculosis* strain H37Rv electrochemical sensor mediated by aptamer and AuNPs−DNA. *ACS Sens.* **2019**, *4*, 849−855.

(10) Bai, L.; Chen, Y.; Liu, X.; Zhou, J.; Cao, J.; Hou, L.; Guo, S. Ultrasensitive electrochemical detection of *mycobacterium tuberculosis* IS6110 fragment using gold nanoparticles decorated fullerene nanoparticles/nitrogen-doped graphene nanosheet as signal tags. *Anal. Chim. Acta* **2019**, *1080*, 75−83.

(11) Saengdee, P.; Chaisriratanakul, W.; Bunjongpru, W.; Sripumkhai, W.; Srisuwan, A.; Hruanun, C.; Poyai, A.; Phunpae, P.; Pata, S.; Jeamsaksiri, W.; Kasinreak, W.; Promptmas, C. A Silicon nitride isfet based immunosensor for Ag85B detection of tuberculosis. *Analyst* **2016**, *141*, 5767.

(12) Tran, D. P.; Pham, T. T. T.; Wolfrum, B.; Offenhäusser, A.; Thierry, B. CMOS-compatible silicon nanowire field-effect transistor biosensor: technology development toward commercialization. *Materials* **2018**, *11*, 785.

(13) Ma, J.; Du, M.; Wang, C.; Xie, X.; Wang, H.; Zhang, Q. Advances in airborne microorganisms detection using biosensors: A critical review. *Front. Environ. Sci. Eng.* **2021**, *15*, 47.

(14) Chen, Y.; Guo, S.; Zhao, M.; Zhang, P.; Xin, Z.; Tao, J.; Bai, L. Amperometric DNA biosensor for *mycobacterium tuberculosis* detection using flower-like carbon nanotubes-polyaniline nanohybrid and enzyme-assisted signal amplification strategy. *Biosens. Bioelectron.* **2018**, *119*, 215−220.

(15) Mogha, N. K.; Sahu, V.; Sharma, R. K.; Masram, D. T. Reduced graphene oxide nanoribbon immobilized gold nanoparticle based electrochemical DNA biosensor for the detection of *mycobacterium tuberculosis*. *J. Mater. Chem. B* **2018**, *6*, 5181−5187.

(16) Cui, F.; Ye, Y.; Ping, J.; Sun, X. Carbon dots: Current advances in pathogenic bacteria monitoring and prospect applications. *Biosens. Bioelectron.* **2020**, *156*, 112085.

(17) Cui, Y.; Zhong, Z.; Wang, D.; Wang, W. U.; Lieber, C. M. High performance silicon nanowire field effect transistors. *Nano Lett.* **2003**, *3*, 149−152.

(18) Ahmad, R.; Mahmoudi, T.; Ahn, M. S.; Hahn, Y. B. Recent advances in nanowires-based field-effect transistors for biological sensor applications. *Biosens. Bioelectron.* **2018**, *100*, 312−325.

(19) Shen, F.; Wang, J.; Xu, Z.; Wu, Y.; Chen, Q.; Li, X.; Jie, X.; Li, L.; Yao, M.; Guo, X.; Zhu, T. Rapid flu diagnosis using silicon nanowire sensor. *Nano Lett.* **2012**, *12*, 3722−3730.

(20) Gao, A.; Lu, N.; Dai, P.; Li, T.; Pei, H.; Gao, X.; Gong, Y.; Wang, Y.; Fan, C. Silicon-nanowire-based CMOS-compatible field-effect transistor nanosensors for ultrasensitive electrical detection of nucleic acids. *Nano Lett.* **2011**, *11*, 3974−3978.

(21) Duan, X.; Gao, R.; Xie, P.; Cohen-Karni, T.; Qing, Q.; Choe, H. S.; Tian, B.; Jiang, X.; Lieber, C. M. Intracellular recordings of action potentials by an extracellular nanoscale field-effect transistor. *Nat. Nanotechnol.* **2012**, *7*, 174−179.

(22) Timko, B. P.; Cohen-Karni, T.; Yu, G.; Qing, Q.; Tian, B.; Lieber, C. M. Electrical recording from hearts with flexible nanowire device arrays. *Nano Lett.* **2009**, *9*, 914−918.

(23) Yang, X.; Chen, S.; Zhang, H.; Huang, Z.; Liu, X.; Cheng, Z.; Li, T. Trace level analysis of nerve agent simulant dmmp with silicon nanowire fet sensor. *IEEE Sens. J.* **2020**, *20*, 12096−12101.

(24) Wipf, M.; Stoop, R. L.; Tarasov, A.; Bedner, K.; Fu, W.; Wright, I. A.; Martin, C. J.; Constable, E. C.; Calame, M.; Schönenberger, C. Selective sodium sensing with gold-coated silicon nanowire field-effect transistors in a differential setup. *ACS Nano* **2013**, *7*, 5978−5983.

(25) Akbari-Saatlu, M.; Procek, M.; Mattsson, C.; Thungström, G.; Nilsson, H. E.; Xiong, W.; Xu, B.; Li, Y.; Radamson, H. H. Silicon nanowires for gas sensing: a review. *Nanomaterials* **2020**, *10*, 2215.

(26) Gao, A.; Lu, N.; Wang, Y.; Dai, P.; Li, T.; Gao, X.; Wang, Y.; Fan, C. Enhanced sensing of nucleic acids with silicon nanowire field effect transistor biosensors. *Nano Lett.* **2012**, *12*, 5262−5268.
(27) Shehada, N.; Cancilla, J. C.; Torrecilla, J. S.; Pariente, E. S.; Brönstrup, G.; Christiansen, S.; Johnson, D. W.; Leja, M.; Davies, M. P. A.; Liran, O.; Peled, N.; Haick, H. Silicon nanowire sensors enable diagnosis of patients via exhaled breath. *ACS Nano* **2016**, *10*, 7047−7057.
(28) Lee, H. S.; Kim, K. S.; Kim, C. J.; Hahn, S. K.; Jo, M. H. Electrical detection of vegfs for cancer diagnoses using anti-vascular endotherial growth factor aptamer-modified si nanowire fets. *Biosens. Bioelectron.* **2009**, *24*, 1801−1805.
(29) Regonda, S.; Tian, R.; Gao, J.; Greene, S.; Ding, J.; Hu, W. Silicon multi-nanochannel fets to improve device uniformity/stability and femtomolar detection of insulin in serum. *Biosens. Bioelectron.* **2013**, *45*, 245−251.
(30) Lin, C.-H.; Hsiao, C.-Y.; Hung, C.-H.; Lo, Y.-R.; Lee, C.-C.; Su, C.-J.; Lin, H.-C.; Ko, F.-H.; Huang, T.-Y.; Yang, Y.-S. Ultrasensitive detection of dopamine using a polysilicon nanowire field-effect transistor. *Chem. Commun.* **2008**, *44*, 5749−5751.
(31) Wang, H.; Chen, S.; Gao, A.; Wang, Y.; Li, T. Detection of TNT in sulfuric acid solution by siNWS-FET based sensor. *Microsyst. Technol.* **2020**, *3*, 1.
(32) Meir, R.; Zverzhinetsky, M.; Harpak, N.; Borberg, E.; Burstein, L.; Zeiri, O.; Krivitsky, V.; Patolsky, F. Direct detection of uranyl in urine by dissociation from aptamer-modified nanosensor arrays. *Anal. Chem.* **2020**, 12528.
(33) Curreli, M.; Zhang, R.; Ishikawa, F. N.; Chang, H.-K.; Cote, R. J.; Zhou, C.; Thompson, M. E. Real-time, label-free detection of biological entities using nanowire-based fets. *IEEE Trans. Nanotechnol.* **2008**, *7*, 651−667.
(34) Kesler, V.; Murmann, B.; Soh, H. T. Going beyond the debye length: overcoming charge screening limitations in next-generation bioelectronic sensors. *ACS Nano* **2020**, *14*, 16194−16201.
(35) Gao, N.; Zhou, W.; Jiang, X.; Hong, G.; Fu, T.-M.; Lieber, C. M. General strategy for biodetection in high ionic strength solutions using transistor-based nanoelectronic sensors. *Nano Lett.* **2015**, *15*, 2143−2148.
(36) Gutiérrez-Sanz, Ó.; Andoy, N. M.; Filipiak, M. S.; Haustein, N.; Tarasov, A. Direct, label-free, and rapid transistor-based immunodetection in whole serum. *Acs Sens.* **2017**, *2*, 1278−1286.
(37) Bhattacharyya, I. M.; Cohen, S.; Shalabny, A.; Bashouti, M.; Akabayov, B.; Shalev, G. Specific and label-free immunosensing of protein-protein interactions with silicon-based immunoFETs. *Biosens. Bioelectron.* **2019**, *132*, 143−161.
(38) Wiker, H. G.; Harboe, M. The antigen 85 complex: a major secretion product of *mycobacterium tuberculosis*. *Microbiol. Rev.* **1992**, *56*, 648−661.
(39) Kashyap, R. S.; Ramteke, S. P.; Deshpande, P. S.; Purohit, H. J.; Taori, G. M.; Daginawala, H. F. Comparison of an adenosine deaminase assay with ELISA for the diagnosis of tuberculous meningitis infection. *Med. Sci. Monit.* **2007**, *13*, BR200−BR204.
(40) Su, D. S.; Chen, P. Y.; Chiu, H. C.; Han, C. C.; Yen, T. J.; Chen, H. M. Disease antigens detection by silicon nanowires with the efficiency optimization of their antibodies on a chip. *Biosens. Bioelectron.* **2019**, *141*, 111209.
(41) Mirsian, S.; Khodadadian, A.; Hedayati, M.; Manzour-ol-Ajdad, A.; Kalantarinejad, R.; Heitzinger, C. A new method for selective functionalization of silicon nanowire sensors and Bayesian inversion for its parameters. *Biosens. Bioelectron.* **2019**, *142*, 111527.
(42) Peláez, E. C.; Estevez, M. C.; Mongui, A.; Menéndez, M. C.; Toro, C.; Herrera-Sandoval, O. L.; Robledo, J.; García, M. J.; Portillo, P. D.; Lechuga, L. M. Detection and quantification of HspX antigen in sputum samples using plasmonic biosensing: toward a real point-of-care (POC) for tuberculosis diagnosis. *ACS Infect. Dis.* **2020**, *6*, 1110−1120.
(43) Holz, O.; Kips, J.; Magnussen, H. Update on sputum methodology. *Eur. Respir. J.* **2000**, *16*, 355−359.
(44) Srivastava, S.; Chapagain, M.; Gumbo, T. Effect of specimen processing, growth supplement, and different metabolic population on *mycobacterium tuberculosis* laboratory diagnosis. *PLoS One* **2020**, *15*, No. e0230927.
(45) Gao, A.; Wang, Y.; Zhang, D.; He, Y.; Zhang, L.; Liu, Y.; Wang, Y.; Song, H.; Li, T. Highly sensitive and selective detection of human-derived volatile organic compounds based on odorant binding proteins functionalized silicon nanowire array. *Sens. Actuators, B* **2020**, *309*, 127762.
(46) Yang, Y.; Lu, Z.; Liu, D.; Wang, Y.; Chen, S.; Li, T. A theoretical and simulation analysis of the sensitivity of SiNWs-FET sensors. *Biosensors* **2021**, *11*, 121.
(47) Jie, J.; Zhang, W.; Peng, K.; Yuan, G.; Lee, C. S.; Lee, S.-T. Surface-dominated transport properties of silicon nanowires. *Adv. Funct. Mater.* **2008**, *18*, 3251−3257.
(48) Shinwari, M. W.; Zhitomirsky, D.; Deen, I. A.; Selvaganapathy, P. R.; Deen, M. J.; Landheer, D. Microfabricated reference electrodes and their biosensing applications. *Sensors* **2010**, *10*, 1679−1715.
(49) Duan, X.; Li, Y.; Rajan, N. K.; Routenberg, D. A.; Modis, Y.; Reed, M. A. Quantification of the affinities and kinetics of protein interactions using silicon nanowire biosensors. *Nat. Nanotechnol.* **2012**, *7*, 401−407.
(50) Israelachvili, J. *Intermolecular and Surface Forces*; 2nd ed. Academic Press: London, 1991.
(51) Stern, E.; Steenblock, E. R.; Reed, M. A.; Fahmy, T. M. Label-Free Electronic Detection of the Antigen-Specific T-Cell Immune Response. *Nano Lett.* **2008**, *8*, 3310−3314.
(52) Deen, M. J.; Shinwari, M. W.; Ranuárez, J. C.; Landheer, D. Noise considerations in field-effect biosensors. *J. Appl. Phys.* **2006**, *100*, No. 074703.
(53) Chu, C.-H.; Sarangadharan, I.; Regmi, A.; Chen, Y.-W.; Hsu, C.-P.; Chang, W.-H.; Lee, G.-Y.; Chyi, J.-I.; Chen, C.-C.; Shiesh, S.-C.; Lee, G.-B.; Wang, Y.-L. Beyond the Debye length in high ionic strength solution: direct protein detection with field-effect transistors (FETs) in human serum. *Sci. Rep.* **2017**, *7*, 5256.
(54) Lloret, N.; Frederiksen, R. S.; Møller, T. C.; Rieben, N. I.; Upadhyay, S.; De Vico, L.; Jensen, J. H.; Nygård, J.; Martinez, K. L. Effects of buffer composition and dilution on nanowire field-effect biosensors. *Nanotechnology* **2013**, *24*, No. 035501.
(55) Stern, E.; Wagner, R.; Sigworth, F. J.; Breaker, R.; Fahmy, T. M.; Reed, M. A. Importance of the Debye screening length on nanowire field effect transistor sensors. *Nano Lett.* **2007**, *7*, 3405.
(56) Kang, Y.; Jiao, S.; Zhao, Y.; Wang, B.; Zhang, Z.; Yin, W.; Tan, Y.; Pang, G. High-flux and high rejection TiO2 nanofibers ultrafiltration membrane with porous titanium as supporter. *Sep. Purif. Technol.* **2020**, *248*, 117000.
(57) Wang, X.; Wang, Y.; Xu, H.; Shan, H.; Lu, J. R. Dynamic adsorption of monoclonal antibody layers on hydrophilic silica surface: A combined study by spectroscopic ellipsometry and AFM. *J. Colloid Interface Sci.* **2008**, *323*, 18−25.
(58) Wang, H.; Chen, S.; Wang, Y.; Li, T. Influence of thickness of SiO_2 layer on the performance of SINW sensors. *Micro Nano Lett.* **2021**, 64−70.
(59) Zhang, N.; Zhang, Z.; Zhang, Q.; Wei, Q.; Zhang, J.; Tang, S.; Lv, C.; Wang, W.; Zhao, H.; Wei, F.; Yan, J.; Baklanov, M.; Yin, H.; Wang, W.; Tu, H. O_2 plasma treated biosensor for enhancing detection sensitivity of sulfadiazine in a high-κ HfO_2 coated silicon nanowire array. *Sens. Actuator, B* **2020**, *306*, 127464.
(60) Chen, C. P.; Ganguly, A.; Lu, C. Y.; Chen, T. Y.; Kuo, C. C.; Chen, R. S.; Tu, W. H.; Fischer, W. B.; Chen, K. H.; Chen, L. C. Ultrasensitive in situ label-free DNA detection using a GaN nanowire-based extended-gate field-effect-transistor sensor. *Anal. Chem.* **2011**, *83*, 1938−1943.
(61) Phunpae, P.; Chanwong, S.; Tayapiwatana, C.; Apiratmateekul, N.; Makeudom, A.; Kasinrerk, W. Rapid diagnosis of tuberculosis by identification of Antigen 85 in mycobacterial culture system. *Diagn. Microbiol. Infect. Dis.* **2014**, *78*, 242.

https://doi.org/10.1021/acssensors.1c01227
ACS Sens. 2021, 6, 3367−3376